Optics Letters

Push—pull microring-assisted space-and-wavelength selective switch

Yishen Huang,[1,*] Qixiang Cheng,[2] Anthony Rizzo,[1] and Keren Bergman[1]

[1]Department of Electrical Engineering, Columbia University, New York, New York 10027, USA
[2]Electrical Engineering Division, Engineering Department, University of Cambridge, 9, JJ Thomson Avenue, Cambridge CB3 0FA, UK
*Corresponding author: y.huang@columbia.edu

Received 11 March 2020; revised 29 March 2020; accepted 6 April 2020; posted 7 April 2020 (Doc. ID 392482); published 5 May 2020

We introduce a novel design of a space-and-wavelength selective switch based on microring-assisted Mach–Zehnder interferometers. Multiple pairs of overcoupled microring resonators are incorporated as efficient and narrowband phase shifters and are driven in push–pull scheme. We design and demonstrate a 2 × 2 × 2λ elementary switch block with full spatial and spectral switching capabilities. The switching device's cross talk suppression and extinction ratio both exceed 21 dB. We measure over 75 GHz optical bandwidth per channel and less than 1.5 dB power penalty at 10^{-9} BER when two 32 Gbps on–off keying signals are loaded simultaneously. This new class of switching elements can further enable compact and high-performance space-and-wavelength selective switch fabrics without the need for wavelength (de)multiplexers or parallel switching planes.

https://doi.org/10.1364/OL.392482

The dramatic growth in the scale and speed of datacenters is the primary driving force for high-bandwidth and low-latency networking solutions. As optical links become the physical medium for inter-rack links in datacenters, dynamic optical connectivity in the form of optical switching can further enable high-performance networking applications such as disaggregated hardware and application-dependent bandwidth allocation [1]. Optical switching technologies have the potential to deliver ultrahigh bandwidth and agile reconfigurability with modulation-agnostic routing [2]. Highly integrated and compact optical switching devices can be realized in silicon photonics owing to high index contrast and well-developed silicon fabrication processes, and large port-count optical switches can be built by assembling thousands of silicon photonic switching elements (SEs) in a network. Recent works on integrated silicon switches have achieved a radix up to 240 × 240 using SEs implemented by micro-electromechanical system (MEMS)-actuated directional couplers (DCs) [3], and a radix up to 64 × 64 with Mach–Zehnder interferometer (MZI)-based SEs [4].

Switching in both spatial and spectral domains is key to further enhance agile optical switching for wavelength division multiplexing (WDM) applications. To perform space-and-wavelength selective switching in devices built with broadband DCs and MZIs, WDM channels need to be first distinguished spatially before being routed. Prior works [5–7] of space-and-wavelength switch designs have introduced parallel switching planes bookended with wavelength (de)multiplexers, but the duplication of switching planes poses immense challenges to managing the complexity and footprint of the integrated systems. In contrast, space-and-wavelength selective switching can be significantly simplified by integrating independent controls for both spatial and spectral domains at the SE level with wavelength selective structures such as microring resonators (MRR) [8], photonic crystal nanobeams [9], and waveguide Bragg gratings [10]. In particular, MRR-based SEs offer promising characteristics of large switching extinction ratio (ER), high tuning efficiency, ultracompact footprint (∼100 μm^2), and commercial manufacturability, which are key factors for scaling to high-radix switch fabrics [8]. Previous works [11,12] for MRR-based space-and-wavelength selective SEs have employed multiple MRRs with offset resonances as spectral add–drop filters. Achieving decent switching ER with add–drop MRRs requires careful examination of the critical-coupling conditions, which, however, are susceptible to fabrication variations. In contrast, overcoupled MRRs as phase shifters tend to have relaxed design constraints, and thus improved tolerance to variations.

In this work, we introduce a novel SE design that we first proposed in Ref. [13] with full space-and-wavelength switching using a symmetrical MZI assisted by pairs of overcoupled MRRs. The MRRs are operated as highly efficient narrowband phase shifters to enable independent switching of multiple wavelengths in the MZI structure. As a demonstration, we design and characterize a 2 × 2 × 2λ SE device, which shows high ER, highly suppressed cross talk, and low signal penalty with a push–pull control scheme when WDM signals are switched simultaneously. Figure 1 shows a generic design of the proposed space-and-wavelength selective SE, independently switching M wavelength channels in an MZI structure with M-pairs of MRRs and a broadband $\pi/2$ phase difference between the arms. The SE maintains a compact footprint by using overcoupled MRRs as efficient phase shifters, which induce a sharp and continuous 2π phase change across their resonances. Each pair of identical MRRs aligns to a specific wavelength channel and operates differentially to create a symmetric MZI passband. By maintaining a two-input and two-output spatial configuration, the SE is a compatible building block for any multistage switch topologies based on 2 × 2 elementary cells [14] and

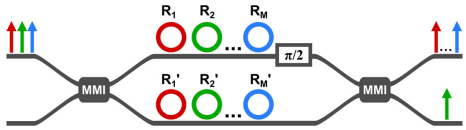

Fig. 1. Schematic of a 2 × 2 × Mλ SE with MRR phase shifters. Each pair of MRRs aligns to the input wavelength channel of the same color.

can be interconnected to scale to larger N × N × Mλ fabrics. Since the MRRs have periodic resonances, the total number of channels supported in a single MZI structure, M, is limited by

$$\mathrm{M} \leq \left\lfloor \frac{\mathrm{FSR}}{\Delta f + \mathrm{FWHM}} \right\rfloor, \tag{1}$$

where FSR and FWHM are, respectively, the free-spectral range and full width at half-maximum transmission of the MRRs, and Δf is the detuning between the pair of MRRs for a single channel.

To illustrate the working principles of the MRR-assisted switching, we examine a single-channel wavelength selective MZI with one pair of MRR phase shifters. This structure, as shown in Fig. 2(a), has been implemented in designs for efficient spatial SEs [15], modulators [16,17], and wavelength interleavers [18]. With one MRR coupled to each arm, the MZI switching phase is achieved by slight detuning of the MRRs' resonances. Figures 2(b) and 2(d) visualize the phase delay induced by the MRRs, as well as the resultant phase differences between the MZI arms in the Bar and Cross switching states, respectively. In this work, we employ the push–pull control scheme for the pair of MRRs around the MZI's quadrature point—the resonances of the MRRs are driven in opposite directions about the switched channel, and a static and wideband phase bias of $\pi/2$ is set between the arms. Under this control scheme, both the Bar and Cross switching states have identical transmission spectra, as shown in Figs. 2(c) and 2(e), and thus eliminate state-dependent performance variations. To route the wavelength channel from Port 1 to Port 3 [Figs. 2(b) and 2(c)], MRR 1 is redshifted from the channel wavelength at zero detuning, while MRR 2 is blueshifted. To route the wavelength channel from Port 1 to Port 4 [Figs. 2(d) and 2(e)], MRR 1 is blueshifted from the channel, while MRR 2 is redshifted.

To demonstrate independent switching of multiple wavelength channels with the proposed switch design, we design and fabricate a 2 × 2 × 2λ SE device that incorporates two pairs of MRRs for simultaneous switching of two wavelength channels. Figure 3(a) shows the micrograph of the device, integrating two multimode interferometers (MMI), four MRRs, and two MZI thermo-optic (TO) tuners under a footprint of 0.17 mm^2. The MRRs have a racetrack shape with an 8 μm bending radius and a 5 μm straight coupling section. The gap between the MRR and bus waveguide is 100 nm, imposing strong overcoupling conditions. Thermal isolation trenches are placed between the two MZI arms to reduce the thermal cross talk between the phase shifters. The MZI tuners and the MRR phase shifters are implemented with TiN heaters to induce localized index change to the silicon waveguides without incurring additional insertion loss (IL). The switch chip is designed and fabricated in a multi-project-wafer (MPW) run through a commercial 200 mm

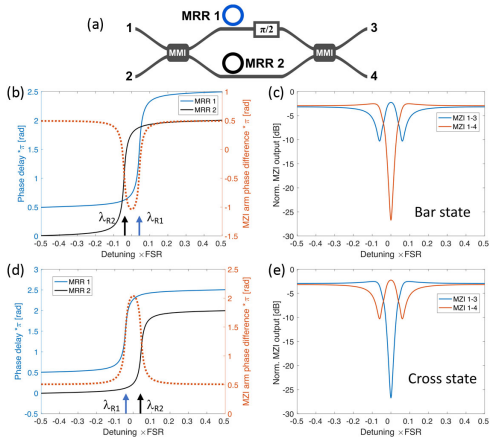

Fig. 2. (a) Schematic of the single-channel MRR-assisted MZI. (b) Induced phase by MRR 1 and MRR 2 and the MZI arms' phase difference for Bar switching state, with center resonances of MRR 1 and MRR 2 labeled as λ_{R1} and λ_{R2}, respectively. (c) Bar-state MZI output spectra for paths Port 1 to Port 3 and Port 1 to Port 4. (d) Induced phase by MRR 1 and MRR 2 and the MZI arms' phase difference for Cross switching state. (e) Cross-state MZI output spectra for paths Port 1 to Port 3 and Port 1 to Port 4.

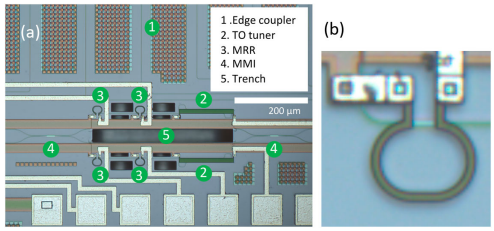

Fig. 3. (a) Micrograph of the 2 × 2 × 2λ SE. (b) MRR heater structure.

silicon-on-insulator (SOI) platform offered by Advanced Micro Foundry.

The fabricated device is accessed optically with TE-polarized light via edge-coupled fiber arrays and electrically via probes. The coupling loss is measured to be ∼3 dB per facet with lensed fibers. The TO phase shifter performances are shown in Figs. 4(a) and 4(b). The MZI tuner shows a tuning efficiency of 13.6 mW/π and results in an MZI ER over 32 dB. The MRR shifter, shown in Fig. 3(b), has a tuning efficiency of 0.262 nm/mW and is used to both align the resonance point and perform switching. Figure 4(c) shows the transmission spectra of the MZI when a single pair of MRRs′, R1 and R1′, are far detuned. We measure the FSR of the MRRs to be 1.182 THz, and the 3 dB bandwidth to be 101 GHz, giving a finesse of 11.7. The switching speed of the switch is measured by applying a 2 V DC bias and a 15 kHz electrical square wave with 175 mV peak-to-peak amplitude to the MRR TO shifter. Observing the power levels of the resonant channel, the 0–90% optical rise and fall times of the MRR output are measured as 13 μs and 12 μs, respectively, as shown in Fig. 4(d).

For switching characterization of the 2 × 2 × 2λ SE, the TO tuner on the top MZI arm is set to a phase bias of $\pi/2$. Two continuous-wave (CW) laser signals at 1537.3 nm and 1541.3 nm, as Channel 1 and Channel 2, respectively, are

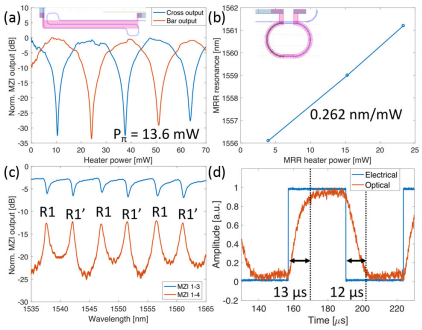

Fig. 4. (a) MZI switching output as a function of TO tuner power consumption; the inset shows the TO tuner design. (b) Resonance tuning power with the TO MRR shifter. (c) Offset MRR resonances while the MZI is biased to Bar state. (d) Optical rise and fall times when the MRR TO shifter is driven with a 15 kHz electrical square wave signal.

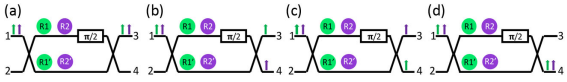

Fig. 5. (a)–(d) Illustrations of (Bar, Bar), (Bar, Cross), (Cross, Bar), and (Cross, Cross) states for the two independently switched channels.

combined before inputting to Port 1 of the SE. We set the resonances of the first MRR pair, R1 and R1′, at Channel 1, and the resonances of the second MRR pair, R2 and R2′, at Channel 2. In contrast to spatial 2 × 2 SE with binary states of Bar and Cross, the space-and-wavelength selective SE supports four switching states—(Bar, Bar), (Bar, Cross), (Cross, Bar), and (Cross, Cross)—for (Channel 1, Channel 2), respectively, as illustrated in Figs. 5(a)–5(d). Each pair of MRRs operates in push–pull for its corresponding channel. To switch a channel to Bar state, the MRR corresponding to that channel on the top arm (R1 or R2) redshifts its resonance with a slight increase of bias on its TO shifter, while the MRR on the bottom arm (R1′ or R2′) blueshifts with a slight decrease in its TO bias, resulting in a π phase difference between the MZI arms at the channel wavelength. To switch a channel to cross state, the top arm's MRR blueshifts while the bottom arm's MRR redshifts, resulting in a 2π phase difference between the MZI arms.

Switch outputs at Port 3 and Port 4 are monitored by an optical spectrum analyzer for the two wavelengths under operation. Figures 6(a)–6(d) show the output channel power levels for Path Port 1–Port 3 and Path Port 1–Port 4 in the four switching states. We observe an average cross talk suppression ratio of 21.7 dB, as indicated in Figs. 6(a)–6(d). The on-chip loss for switched signal averages to 5.1 dB, which is due to a combination of MMI loss and intensity modulation by the MRRs in the overcoupling regime. For a specific wavelength channel, we define the switching ER as the difference between the signal power of the channel in one state and the leakage power of the same channel switched to other states. For instance, the ER for the Channel 1 in Bar is determined by the average signal power at 1537.3 nm between states (Bar, Bar) and (Bar, Cross), subtracted by the average leakage power for Channel 1 between states (Cross, Bar) and (Cross, Cross). Between the two channels, we measure an average ER of 21.8 dB for Bar state, and 21.6 dB for Cross state. Figures 6(e)–6(h) show the output spectra of all switching states measured with a broadband source. The signal passbands of

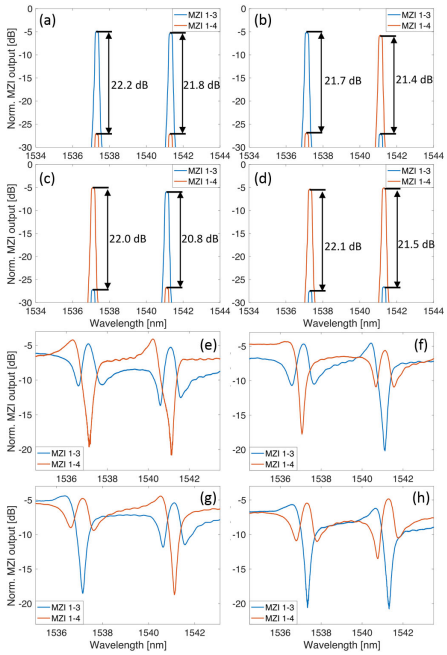

Fig. 6. (a)–(d) Signal and leakage power levels with two CW lasers in the four switching states. Cross talk suppression levels are indicated. (e)–(h) Transmission spectra for both switch paths in the four switching states.

both channels in all switching states are fairly consistent and average to 75.1 GHz.

We numerically simulate the 2 × 2 × 2λ SE using the transfer matrix method [15] to optimize for the cross talk suppression and IL during switching. In this analysis, the two wavelength channels are spaced at $\Delta f + \mathrm{FWHM}$—the closest spacing defined by Eq. (1). We maintain the experimentally extracted value for the MRR's finesse, $\mathcal{F}$, which is a function of the product between the MRRs' self-coupling coefficient, r, and round trip amplitude transmission, a,

$$\mathcal{F} = \frac{\mathrm{FSR}}{\mathrm{FWHM}} = \frac{\pi\sqrt{ra}}{1-ra}. \tag{2}$$

We examine the MRR detuning between 10%–40% of their FSR and a valued between 0.875 and 0.993, with corresponding r values to maintain a finesse of 11.7. The sweep in a can inform how to better design the intrinsic loss of the MRRs, while the sweep in MRR detuning can inform more precise push–pull control. For instance, it is possible to achieve >25 dB cross talk suppression and <1 dB IL with $a = 0.96$ and MRRs detuned between 19% and 22% of their FSR, as indicated by the line markers in Figs. 7(a) and 7(b). Further improvements in cross talk suppression beyond 35 dB and IL below 0.5 dB are possible by increasing both a and the MRRs' detuning, making the device comparable to state-of-art high performance silicon switches [19,20] and viable for scaling to higher port counts with multistage wavelength selective switch topologies.

Data transmission was performed for switching states (Bar, Cross) and (Cross, Bar), where the two wavelength channels are launched into the same input port but switched to different output ports. A total of four switched signals are examined: (Bar, Cross)-Channel 1, (Bar, Cross)-Channel 2, (Cross, Bar)-Channel 1, (Cross, Bar)-Channel 2. We examine the switching

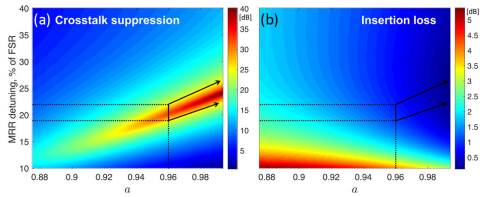

Fig. 7. (a) Cross talk suppression and (b) IL over ranges of MRR detuning and round trip amplitude transmission.

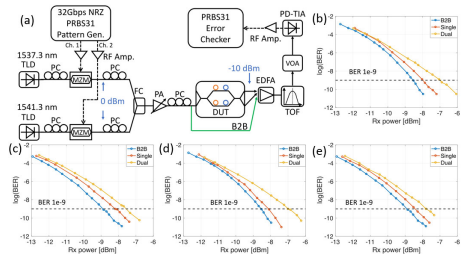

Fig. 8. (a) Data experiment setup schematic. TLD, tunable laser diode; PC, polarization controller; DUT, device under test. (b)–(e) BER curve for switching states (Bar, Cross)-Channel 1, (Bar, Cross)-Channel 2, (Cross, Bar)-Channel 1, and (Cross, Bar)-Channel 2, respectively, compared among B2B, single-, and dual-channel cases.

states with one or both channels transmitting (single- or dual-channel cases) to study the impact of interchannel cross talk on the data routing performance. The data test schematic is shown in Fig. 8(a). An Anritsu MP1900A Signal Quality Analyzer generates two electrically decorrelated signals at 32 Gbps non-return-to-zero (NRZ) on–off keying (OOK) using $2^{31}-1$ pseudo-random bit sequence (PRBS31). Two optical carriers at 1537.3 nm and 1541.3 nm are modulated by Mach–Zehnder modulators (MZM) with 0 dBm output power and combined using a fiber coupler (FC) before entering the silicon photonic chip. A power adjuster (PA) consisting of a variable attenuator (VOA) and an erbium-doped fiber amplifier (EDFA) is used before the switch to compensate for coupling and propagation losses through the chip and ensure −10 dBm of optical power exits the chip. This PA is also used to replicate the device IL in the back-to-back (B2B) reference case. A second set of EDFA and VOA adjusts the receiver optical power for the bit error rate (BER) measurement. A tunable optical filter (TOF) with a passband covering both wavelength channels is used to reject out-of-band amplified spontaneous emission (ASE) noise. The receiver consists of a Finisar XPDV3120 PD-transimpedance-amplifier (TIA) assembly, which performs the optical-to-electrical conversion and allows the data signal to be analyzed by the Anritsu error checker. For each switch path, the cross talk channel is off for the single-channel case, and on for the dual-channel cases. Evident from Figs. 8(b)–8(e), all switch paths' dual-channel cases are within 1 dB power penalty at 10^{-9} BER compared to their single-channel cases without interchannel cross talk, and within 1.5 dB power penalty compared to the B2B reference case.

Space-and-wavelength selective switching can be simplified significantly by integrating spatial and spectral control granularity at the SE level. In this work, we introduce an MRR-assisted MZI SE that achieves independent switching of wavelength channels by using multiple pairs of MRRs as push–pull phase shifters. We discuss the working principles of the design and demonstrate a $2 \times 2 \times 2\lambda$ switch block experimentally. The SE switches two wavelength channels independently in a total of four switching states, with both cross talk suppression and switching ER exceeding 21 dB. Less than 1 dB signal power penalty is observed from interchannel cross talk when transmitting 32 Gbps NRZ data signals. We further show a path to achieve >25 dB cross talk suppression and <1 dB IL through optimizing the MRR intrinsic loss and more precise push–pull control. The SE's high performance, compact footprint, and efficient control make this design a promising building block for scaling to multistage space-and-wavelength selective optical switch fabrics.

Funding. Advanced Research Projects Agency - Energy (ENLITENED (DEAR00000843)); Air Force Research Laboratory (FA8650-15-2-5220).

Disclosures. The authors declare no conflicts of interest.

REFERENCES

1. Y. Shen, X. Meng, Q. Cheng, S. Rumley, N. Abrams, A. Gazman, E. Manzhosov, M. Glick, and K. Bergman, J. Lightwave Technol. **37**, 245 (2019).
2. Q. Cheng, S. Rumley, M. Bahadori, and K. Bergman, Opt. Express **26**, 16022 (2018).
3. T. J. Seok, K. Kwon, J. Henriksson, J. Luo, and M. C. Wu, Optica **6**, 490 (2019).
4. T. Chu, L. Qiao, W. Tang, D. Guo, and W. Wu, *Optical Communication Conference (OFC)* (2018), paper Th1J.4.
5. R. Stabile, A. Rohit, and K. A. Williams, J. Lightwave Technol. **32**, 201 (2014).
6. T. J. Seok, J. Luo, Z. Huang, K. Kwon, J. Henriksson, J. Jacobs, L. Ochikubo, R. S. Muller, and M. C. Wu, *Conference on Lasers and Electro-Optics (CLEO)* (2018), paper STu4B.1.
7. Q. Cheng, M. Bahadori, M. Glick, and K. Bergman, *Conference on Lasers and Electro-Optics (CLEO)* (2019), paper STh1N.4.
8. Q. Cheng, M. Bahadori, Y.-H. Hung, Y. Huang, N. Abrams, and K. Bergman, J. Sel. Top. Quantum Electron. **25**, 3600111 (2019).
9. H. Zhou, C. Qiu, X. Jiang, Q. Zhu, Y. He, Y. Zhang, Y. Su, and R. Soref, Photon. Res. **5**, 108 (2017).
10. R. A. Soref, F. De Leonardis, and V. M. N. Passaro, Opt. Express **26**, 14959 (2018).
11. A. S. P. Khope, M. Saeidi, R. Yu, X. Wu, A. M. Netherton, Y. Liu, Z. Zhang, Y. Xia, G. Fleeman, A. Spott, S. Pinna, C. Schow, R. Helkey, L. Theogarajan, R. C. Alferness, A. A. M. Saleh, and J. E. Bowers, Opt. Express **27**, 5203 (2019).
12. T. Dai, G. Wang, X. Guo, C. Bei, J. Jiang, W. Chen, Y. Wang, H. Yu, and J. Yang, IEEE Photon. Technol. Lett. **30**, 1044 (2018).
13. Y. Huang, Q. Cheng, A. Rizzo, and K. Bergman, *Optical Communication Conference (OFC)* (2020), paper Th2A.7.
14. Q. Cheng, Y. Huang, H. Yang, M. Bahadori, N. Abrams, X. Meng, M. Glick, Y. Liu, M. Hochberg, and K. Bergman, IEEE J. Sel. Top. Quantum Electron. **26**, 8302010 (2020).
15. L. Lu, L. Zhou, X. Li, and J. Chen, Opt. Lett. **39**, 1633 (2014).
16. C.-M. Chang, G. de Valicourt, S. Chandrasekhar, and P. Dong, J. Lightwave Technol. **35**, 3116 (2017).
17. J. Cardenas, P. A. Morton, J. B. Khurgin, A. Griffith, C. B. Poitras, K. Preston, and M. Lipson, Opt. Express **21**, 22549 (2013).
18. Z. Wang, S.-J. Chang, C.-Y. Ni, and Y. J. Chen, IEEE Photon. Technol. Lett. **19**, 1072 (2007).
19. K. Suzuki, R. Konoike, J. Hasegawa, S. Suda, H. Matsuura, K. Ikeda, S. Namiki, and H. Kawashima, J. Lightwave Technol. **37**, 116 (2019).
20. Q. Cheng, L. Y. Dai, N. C. Abrams, Y.-H. Hung, P. E. Morrissey, M. Glick, P. O'Brien, and K. Bergman, Photon. Res. **7**, 155 (2019).